Zero- and one-dimensional thioindates synthesized under solvothermal conditions yielding α-In$_2$S$_3$, β-In$_2$S$_3$ or MgIn$_2$S$_4$ as thermal decomposition products

E. Quiroga-González [a], L. Kienle [b], C. Näther [a], V.S.K. Chakravadhanula [b], H. Lühmann [a], W. Bensch [a,*]

[a] Institute for Inorganic Chemistry of the University of Kiel, Max-Eyth-Str. 2, 24118 Kiel, Germany
[b] Institute of Material Science of the University of Kiel, Synthesis and Real Structure, Kaiserstr. 2, 24143 Kiel, Germany

ARTICLE INFO

ABSTRACT

The first cationic thioindate with composition [In(en)$_2$S]$_2$·2Cl (zero-dimensional) (1) and the first thioindate being charge compensated by a main group metal complex with composition [Mg(en)$_3$]-[In$_2$S$_4$] (one-dimensional) (2) have been prepared with ethylenediamine under solvothermal conditions. The main structural motif of [In(en)$_2$S]$_2$·2Cl is the centro-symmetric rhomboidal [In(en)$_2$S]$_2^{2+}$ ring which is formed by S–S edge-sharing of two symmetry related [InN$_4$S$_2$] octahedra. The structure of [Mg(en)$_3$][In$_2$S$_4$] is composed of a straight one-dimensional $\{[InS_2]^-\}_\infty$ chain surrounded by [Mg(en)$_3$]$^{2+}$ complexes. Both compounds are wide band-gap semiconductors. The thermal decomposition reaction of [In(en)$_2$S]$_2$·2Cl stopped at 500 °C yielded cubic α-In$_2$S$_3$ and reflections of β-In$_2$S$_3$ are seen in the X-ray powder pattern of the residue obtained at 900 °C. In the case of [Mg(en)$_3$][In$_2$S$_4$] the thiospinel MgIn$_2$S$_4$ was identified as decomposition product. The size of the MgIn$_2$S$_4$ crystals are in the nanometer range as evidenced by a pronounced broadening of the reflections in the powder pattern and with transmission electron microscopy.

© 2010 Elsevier Inc. All rights reserved.

1. Introduction

Inorganic–organic hybrid chalcogeno-indates are mainly prepared under solvothermal conditions in the presence of an organic amine as a structure-directing agent. The structures are usually based on the [InQ$_4$] tetrahedra (Q=S, Se, Te) which are interconnected to form supertetrahedral clusters (Tn) as building units [1], or some variants like pentasupertetrahedral [2,3] and capped supertetrahedral clusters [4], respectively. Chalcogeno-indates with structures containing other building units are rare, cf. the compounds [(C$_3$H$_7$)$_2$NH$_2$]$_3$[In$_6$S$_{11}$H] ((C$_3$H$_7$)$_2$NH=dipropylamine) [5] and [C$_{13}$H$_{28}$N$_2$]$_{6.5}$[In$_{33}$S$_{56}$] (C$_{13}$H$_{26}$N$_2$=4,4′-trimethylenedipiperidine) [6]. The structure of the first is composed of [In$_6$S$_{11}$] chains linked by edge-sharing [InS$_4$] tetrahedra [5], while the structure of the second compound is a three-dimensional framework constructed from the cross-linking of helical chains of corner-sharing [InS$_4$] tetrahedra [6]. Recently, a one-dimensional (1-D) thioindate with composition [C$_{10}$N$_4$H$_{26}$]$_{0.5}$[InS$_2$] (C$_{10}$N$_4$H$_{24}$= 1,4-bis(3-aminopropyl)piperazine) was reported, which contains one-dimensional $\{[InS_2]^-\}_\infty$ chains formed by edge-linked [InS$_4$] tetrahedra [7]. Other 1-D thioindates like [Ni(dien)$_2$]$_{0.5}$[InS$_2$] (dien=diethylenetriamine) and [Ni(dap)$_3$]$_{0.5}$[InS$_2$] (dap=1, 2-diaminopropane) have the same $\{[InS_2]^-\}_\infty$ chains, but are

charge-compensated with complexes of transition metals [8]. Recently, cationic inorganic–organic hybrid seleno-indates have been also reported, namely ([In(en)$_2$Se]$_2$·2I and [In(teta)Se]$_2$·2I, en= ethylenediamine, teta=triethylenetetramine) [9]. These compounds are composed of isolated clusters and hence they may be regarded as zero-dimensional (0-D) with respect to the clusters' substructure.

Besides these hybrid compounds the binary inorganic compound In$_2$S$_3$ is in the focus of research because it may replace toxic CdS buffer layers in highly efficient solar cells [10,11]. Additionally, the crystal structures of α- or β-In$_2$S$_3$ present a large amount of vacancies that can serve as host for a number of metal ions to form semiconducting and/or magnetic materials [12]. These structural and chemical features distinguish In$_2$S$_3$ from II/VI compounds, which tend to expel guest ions [13], and offer possibilities for tuning the optical and electrical properties according to the type and concentration of the guest cations. For example, the optical band gap can be continuously tuned when In cations are partially replaced by a metal cation like Cu$^+$ or Na$^+$ [14,15], thus obtaining compounds with formulas [In$_{16}$]$_O$[In$_{5.23-x/3}$ M_xh$_{2.67-2x/3}$]$_T$S$_{32}$ where M is the substituting metal, h represents the vacant sites and T and O be a symbol of the tetrahedral and octahedral sites, respectively. The maximum substitution level is achieved for MIn$_5$S$_8$ with $x\sim4$ [16].

For In$_2$S$_3$ or its derivatives, the optical, electronic and catalytic properties can be adjusted by the size and shape of the crystals [13,17]. Nanocrystalline In$_2$S$_3$ has been prepared applying a wide range of methods like hydrothermal synthesis [17–19], solution

reactions [13,20] and pyrolysis of single source molecular compounds [21] producing either the cubic (α) modification [22,23] or the tetragonal (β) modification [13,18,24]. Among these approaches the use of single molecular source precursors is most studied. Frequently, the synthesis of such precursors is simple and they contain the elements of the desired product homogenously distributed on an atomic scale; however, the size of the organic molecules should be small to keep the contamination with organic constituents as low as possible when fabrication techniques like pyrolysis or thermal decomposition are used.

In our ongoing work in the field of solvothermal synthesis of thiometalate compounds we synthesized a 0-D thioindate with composition $[In(en)_2S]_2 \cdot 2Cl$ (1) and the 1-D thioindate $[Mg(en)_3]$ $[In_2S_4]$ (2). The two compounds were tested as precursors for the preparation of In_2S_3 and $MgIn_2S_4$ using thermal decomposition in inert atmosphere. $MgIn_2S_4$ was obtained in nanocrystalline form whereas good crystalline α-In_2S_3 was obtained as decomposition product of 1. In the paper, the syntheses, crystal structures, thermal and optical properties of the two compounds are reported. The nanocrystals were investigated with transmission electron microscopy (TEM) and X-ray powder diffractometry.

2. Experimental section

2.1. Synthesis of ($[In(en)_2S]_2 \cdot 2Cl$) (1)

For the solvothermal synthesis 0.7 mmol of In and 0.7 mmol of S were used. The precursors were mixed with 4.75 mL of en (ethylenediamine) and 0.25 mL CH_2Cl_2 in a 35 mL Teflon-lined stainless steel autoclave. The sealed vessel was then heated at 190 °C for 5 days. After cooling down to room temperature, the product was filtered off, and washed first with ethanol and then with acetone. Colorless needles in a yield of around 40% based on In were obtained. Performing syntheses with HCl (0.5 mL, concentrated) as chlorine source were also successful (Fig. S1, supporting information). The yield of the compound was comparable with that obtained with CH_2Cl_2. C–H–N–S analysis (in %): Calculated: C, 15.88; H, 5.33; N, 18.52; S, 10.60. Measured: C, 16.02; H, 5.36; N, 18.28; S, 10.45. The FTIR spectrum of the compound exhibits the characteristic peaks for en at 506 (m), 1038 (s), 1100 (m), 1324 (w), 1382 (vw), 1452 (w), 1576 (m), 1631 (vw), 2937 (w) and 3116 cm^{-1} (w). Additionally, the presence of hydrogen bonds is evidenced by the peaks at 3238 (s) and 3425 cm^{-1} (s).

2.2. Synthesis of ($[Mg(en)_3][In_2S_4]$) (2)

This compound was prepared using 0.52 mmol of Mg, 1 mmol of In and 2.1 mmol of S. The starting materials were mixed with 4 mL of en in a 35 mL Teflon-lined stainless steel autoclave. The sealed vessel was then heated at 190 °C for 10 days. After cooling down to room temperature, the product was filtered off, and washed with ethanol and acetone. Prismatic colorless crystals in a yield larger than 80% based on In were obtained. C–H–N–S analysis (in %): Calculated: C, 12.81; H, 4.30; N, 14.94; S, 22.80. Measured: C, 12.17; H, 4.24; N, 14.04; S, 22.78. The FTIR spectrum of this compound presents also the characteristic peaks for en: 494 (m), 1009 (s), 1108 (m), 1337 (w), 1392 (vw), 1453 (w), 1572 (m), 1641 (vw), 2920 (w) and 3138 cm^{-1} (w). The presence of hydrogen bonds is evidenced with the peaks at 3236 (s) and 3285 cm^{-1} (s).

2.3. Thermal decomposition of 1 and 2

Compounds 1 and 2 were crushed and the obtained powders were thermally treated in Argon atmosphere at a rate of 2 °C/min

until 500 °C yielding dark red powders. For descriptive purposes, the powders are named 1x (from compound 1) and 2x (from compound 2). 1x contains 6.48 wt% of organic residue (C–H–N analysis (in %): C, 4.91; H, 0.0; N, 1.57), and 2x contains 2.63 wt% (C–H–N analysis (in %): C, 1.9; H, 0; N, 0.73). Because the weight loss of compound 1 was not finished until 500 °C a second experiment was done with the final temperature of 900 °C. In the residue no C, H or N could be detected with elemental analysis.

2.4. Characterization methods

X-ray single-crystal analysis of 1 and 2 were performed using an Imaging Plate Diffraction System (IPDS1) from Stoe & CIE with Mo$K\alpha$ radiation). The raw data were corrected for Lorentz-polarization effects. The structures were solved with Direct Methods using SHELXS-97 [25]. Structure refinement was performed with SHELXL-97 [25]. All non-hydrogen atoms were refined with anisotropic displacement parameters. All hydrogen atoms were positioned with idealized geometry and refined isotropically using a riding model. For 2, The C–H and N–H atoms were positioned with idealized geometry and also refined using a riding model. In this compound both crystallographically independent en molecules are disordered over two positions. Selected crystal data and results of the structure refinements of 1 and 2 are summarized in Table 1. Selected bond lengths and angles of the structures are shown in Tables 2 (1) and 3 (2).

Crystallographic data (excluding structure factors) have been deposited with the Cambridge Crystallographic Data Center as supplementary publication no. CCDC 794622 and 794623. Copies of the data can be obtained, free of charge via www.ccdc.cam.ac.uk/data_request/cif.

DTA-TG measurements of 1 and 2 were performed in Al_2O_3 crucibles using a STA-409CD thermobalance from Netzsch.

Table 1
Selected data, technical details of data collection and of the refinement results for compounds 1 and 2.

	Compound 1	Compound 2
Empirical formula	$C_8H_{32}Cl_2In_2N_8S_2$	$C_6H_{12}In_2MgN_6S_4$
Formula weight/gr	605.08	550.41
Color	Colorless	Colorless
Crystal size/mm^3	$0.11 \times 0.09 \times 0.07$	$0.1 \times 0.08 \times 0.08$
Crystal system	Monoclinic	Orthorhombic
Space group	$P2_1/n$	$Cmcm$
a/Å	6.4859(3)	9.7196(7)
b/Å	11.1962(9)	15.1887(10)
c/Å	14.2509(8)	13.1473(7)
β/deg	93.763	90
Volume/Å^3	1032.63(11)	1940.9(2)
Z	4	4
Density (calculated)/mg/m^3	1.946	1.884
Wavelength/Å	0.71073	0.71073
Absorption coefficient/mm^{-1}	2.702	2.833
$F(000)$	600	1056
Reflections collected	9459	13834
Independent reflections	2423 [R(int)=0.0339]	1239 [R(int)=0.0365]
Completeness to theta=28.03°	97.0%	96.0%
Data/restraints/parameters	2423/0/101	1239/0/73
Goodness-of-fit on $F2$	1.027	1.129
Final R indices [$I > 2\text{sigma}(I)$]	R1=0.0213, wR2=0.0532	R1=0.0285, wR2=0.0785
R indices (all data)	R1=0.0249, wR2=0.0544	R1=0.0335, wR2=0.0806
Extinction coefficient	0.0073(6)	0.0015(3)
Largest diff. peak and hole/e Å^{-3}	0.760 and −0.767	0.843 and −0.731

Table 2

Selected bond lengths (Å) and angles (deg.) for compound **1**.

In(1)-N(1)	2.3078(17)	In(1)-N(2)	2.4110(17)
In(1)-N(11)	2.3184(18)	In(1)-S(1)#1	2.4731(5)
In(1)-N(12)	2.3330(18)	In(1)-S(1)	2.5040(5)
N(1)–In(1)–N(11)	88.14(6)	N(2)–In(1)–S(1)#1	94.03(4)
N(1)–In(1)–N(12)	151.56(6)	N(1)–In(1)–S(1)	101.06(4)
N(11)–In(1)–N(12)	75.84(7)	N(11)–In(1)–S(1)	88.27(4)
N(1)–In(1)–N(2)	74.60(6)	N(12)–In(1)–S(1)	101.76(4)
N(11)–In(1)–N(2)	84.20(6)	N(2)–In(1)–S(1)	171.39(5)
N(12)–In(1)–N(2)	80.44(6)	S(1)#1–In(1)–S(1)	93.882(15)
N(1)–In(1)–S(1)#1	96.97(4)	In(1)#1–S(1)–In(1)	86.118(15)
N(11)–In(1)–S(1)#1	173.96(5)	C(1)–N(1)–In(1)	112.47(12)
N(12)-In(1)–S(1)#1	98.18(5)	C(2)–N(2)–In(1)	106.22(13)
C(12)-N(12)–In(1)	110.21(13)	C(11)–N(11)–In(1)	106.62(13)

Table 3

Bond lengths [Å] and angles [deg] for compound **2**.

In(1)-S(1)	2.4477(12)	S(1)-In(1)#2	2.4477(12)
In(1)-S(3)	2.4745(9)	S(2)-In(1)#2	2.4773(11)
In(1)-S(3)#1	2.4745(9)	S(3)-In(1)#1	2.4745(9)
In(1)-S(2)	2.4773(11)		
In(1)-In(1)#1	3.2647(6)	S(2)–In(1)–In(1)#1	138.01(3)
S(1)–In(1)–S(3)	113.364(19)	S(1)–In(1)–In(1)#2	47.20(3)
S(1)–In(1)–S(3)#1	113.364(19)	S(3)–In(1)–In(1)#2	131.014(18)
S(3)–In(1)–S(3)#1	97.45(4)	S(3)#1–In(1)–In(1)#2	131.014(18)
S(1)–In(1)–S(2)	95.04(4)	S(2)–In(1)–In(1)#2	47.83(2)
S(3)–In(1)–S(2)	119.360(18)	In(1)#1–In(1)–In(1)#2	174.157(11)
S(3)#1–In(1)–S(2)	119.360(18)	In(1)–S(1)–In(1)#2	85.59(5)
S(1)–In(1)–In(1)#1	126.95(3)	In(1)#2–S(2)–In(1)	84.33(5)
S(3)–In(1)–In(1)#1	48.726(18)	In(1)–S(3)–In(1)#1	82.55(4)
S(3)#1–In(1)–In(1)#1	48.726(18)		

The measurements were performed in Al_2O_3 crucibles under an Argon atmosphere with a heating rate of 2 °C/min. C–H–N–S analysis was performed using a EURO EA Elemental Analyzer by EURO VECTOR Instruments and Software. Additionally, MIR spectra (450–3000 cm^{-1}) were recorded with a spectrometer ATI Mattson Genesis.

UV/vis spectroscopic investigations were conducted at room temperature using a UV/vis-NIR two-channel spectrometer Cary 5 from Varian Techtron Pty., Darmstadt. The optical properties of the compounds were investigated by studying the UV/vis reflectance spectrum of the powdered samples. The absorption data were calculated with the Kubelka–Munk relation for diffuse reflectance data. $BaSO_4$ powder was used as reference material.

The starting materials and thermal decomposition products were investigated with X-ray powder diffractommetry (Stoe STADI P diffractometer, Ge monochromator, Cu$K\alpha$ radiation, $\lambda = 1.54056$ Å). For transmission electron microscopy (TEM) investigations, the powders obtained after thermal annealing of the thioindates were transferred to aluminum grids which were fixed in a side-entry, double-tilt holder with the tilting limited to a maximum of $\pm 25°$ in two directions. High resolution transmission electron microscopy (HRTEM) was performed with a Philips CM30ST (300 kV, LaB$_6$ cathode). EDX (energy dispersive X-ray spectroscopy) was conducted in the scanning and nanoprobe mode of the CM30ST instrument using a Si/Li-EDX detector (Noran, Vantage System).

3. Description of the structure of the thioindates

3.1. Structure of [In(en)$_2$S]$_2$·2Cl (**1**)

Compound **1** consists of zero-dimensional (0-D) thioindate clusters (Fig. 1) crystallizing in the monoclinic space group $P2_1/n$
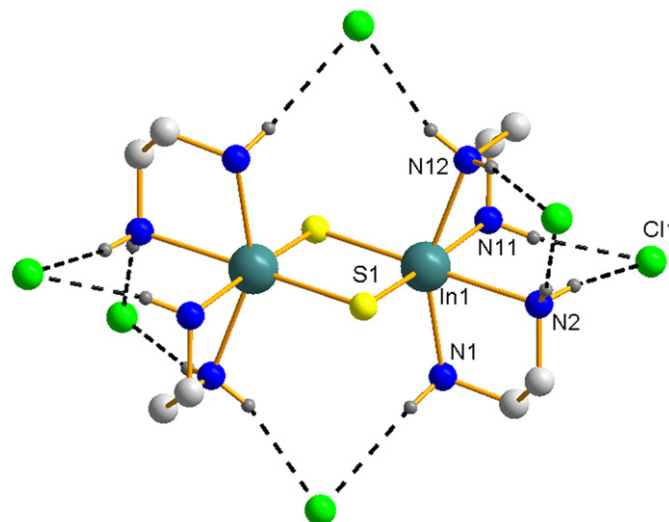
Fig. 1. The central [In(en)$_2$S]$_2^{2+}$ core with atom numbering and its surrounding by Cl$^-$ anions. Note that H-atoms are not numbered and dotted lines indicate N–H$\cdots$Cl interactions.

with all atoms being located on general positions. The In^{3+} cation is coordinated by four N atoms of two en molecules and two S^{2-} anions in a slightly distorted octahedral geometry. The In–N bond lengths ranging from 2.3078(1) to 2.4110(17) Å are significantly longer than in e.g. {[In($C_6H_{14}N_2$)$_2$]$_2$Sb$_4$S$_8$}Cl$_2$ (2.272–2.299 Å) [26], In$_2$Ge$_6$O$_{15}$(en)$_2$ (2.261–2.285 Å) [27], [In(APTSC)$_2$](PF$_6$) (2.230–2.297 Å; APTSC=2-acetylpyridine-thiosemicarbazone) [28] or [HB(2,5-Me$_2$pz)$_3$]In(S$_4$)(3,5-Me$_2$pzH) (2.271–2.341 Å; pz=pyra-zolyl) [29], but are in the range reported for {O[In(HDAPTSC)(OH)]$_2$}·5MeOH (2.292–2.391 Å) (HDAPTSC=2-acetylpyridine-thiosemicarbazone) [28], [In(en)$_2$Se]$_2$·2I (2.309–2.410 Å) [9] and [In(teta)Se]$_2$·2I (2.313–2.368 Å) [9]. The In–S bonds of 2.4731 and 2.5040 Å are comparable with those determined for the above mentioned S-containing compounds or [DEAH]$_7$[In$_{11}$S$_{21}$H$_2$] [30].

The distortion of the [InN$_4$S$_2$] octahedron is obvious analyzing the *trans*-angles that vary from 151.56(6)° to 173.96(5)° and the *cis*-angles ranging between 74.60(6)° and 101.76(4)° (Table 2). The cationic [In(en)$_2$S]$_2^{2+}$ core is constructed by edge-sharing of two symmetry related [InN$_4$S$_2$] octahedra via the S–S edge forming a centro-symmetric rhomboidal In$_2$S$_2$ ring. The two cationic seleno-indates [In(en)$_2$Se]$_2$·2I and [In(teta)Se]$_2$·2I have been previously reported [9] and compound **1** which is isostructural to the former compound represents the first cationic thioindate. Charge compensation is achieved by Cl$^-$ anions and each [In(en)$_2$S]$_2^{2+}$ cation is surrounded by six Cl$^-$ anions (Fig. 1). The Cl$^-$ ions are connected to the central structural motif via weak H-bonds (Cl$\cdots$H distances ranging from 2.32 to 2.94 Å with corresponding N–H$\cdots$Cl angles between 157.22° and 168.25°). The complexes of **1** are linked into chains that run parallel to the [100] direction through N–H$\cdots$S hydrogen bonding interactions (S$\cdots$H distances: 2.40–2.74 Å), as shown in Fig. 2. The extended S$\cdots$H and Cl$\cdots$H interactions generate a three-dimensional framework (Fig. 3). Each [In(en)$_2$S]$_2^{2+}$ cation is surrounded by six further [In(en)$_2$S]$_2^{2+}$ groups generating tunnels along [100] hosting the Cl$^-$ anions.

3.2. Structure of [Mg(en)$_3$][In$_2$S$_4$] (**2**)

The 1-D thioindate **1** crystallizes in the orthorhombic space group *Cmcm* with In, Mg, S and N atoms being located on special positions. The structure consists of linear 1-D {[InS$_2$]$^-$}$_\infty$ chains that run parallel to the [001] direction (Fig. 4). The chains are

formed by [InS$_4$] tetrahedra sharing opposite edges (In–S bond lengths: 2.47 and 2.50 Å, Table 2) with S–In–S angles ranging from 95.04(4)° to 119.36(18)°, significantly deviating from the tetrahedral geometry. The connection mode generates In$_2$S$_2$ rings and neighboring rings are rotated by 90° to each other. The shortest In–In distance of 3.265 Å and the other geometric parameters are similar to those reported for other 1-D thioindates [7,8]. An identical linkage mode of MQ_4 tetrahedra is observed for SiS$_2$ [31] or K$_2$HgSnTe$_4$ [32].

The polymeric anion is charge compensated by a [Mg(en)$_3$]$^{2+}$ complex (Fig. 5a). There have been some reports about 1-D thioindates charge-compensated with protonated amine molecules [7] and with transition metal complexes [8], but this is the first time that charge compensation is achieved by an earth-alkaline metal complex. The Mg–N bond lengths of 2.20 and 2.22 Å are comparable with data recently published for [Mg(en)$_3$][Sb$_4$S$_7$] in [33]. Like in the thioantimonate, the octahedral environment around Mg^{2+} is strongly distorted as evidenced by the N–Mg–N angles (see Table 3).

The linear chains are arranged on a rectangular net with channels running along [001] being occupied by the [Mg(en)$_3$]$^{2+}$ complexes (Fig. 5b). The structure of **2** is stabilized by numerous weak N–H···S H-bonds (bond lengths ranging from 2.55 to 2.98 Å) between the Mg complexes and the anionic chains.

4. Thermal and optical characterization of the thioindates

4.1. Thermal properties

The homogeneity of the compounds was proved with X-ray powder diffractometry (Fig. S2, supporting information). The DTA and TG curves of compounds **1** and **2** are shown in Fig. 6(a) and (b). According to the TG curve compound **1** undergoes a complex decomposition process with endothermic events in the DTA curve with T_{onset} values indicated in Fig. 6a. A straightforward
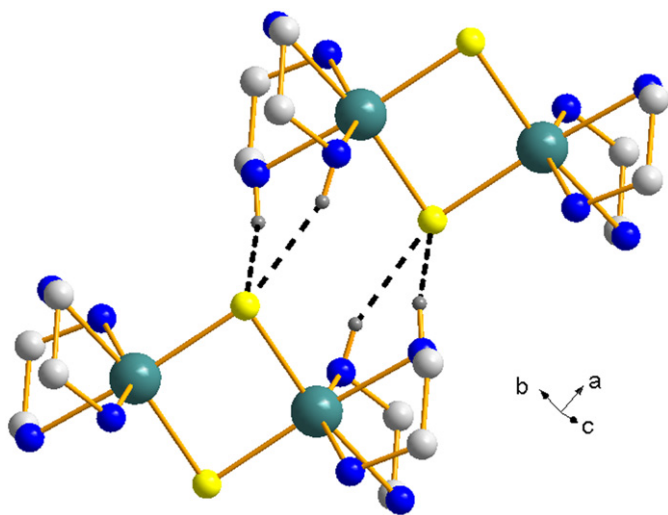
Fig. 2. The S···H bonding interactions (dotted lines) in **1** generating chains running along the [100] direction.
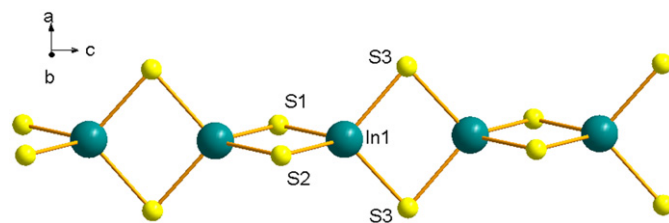
Fig. 4. 1-D {[InS$_2$]$^-$}$_\infty$ chain of **2**, which runs parallel to the [001] direction. It is composed of edge-sharing [InS$_4$] tetrahedra.

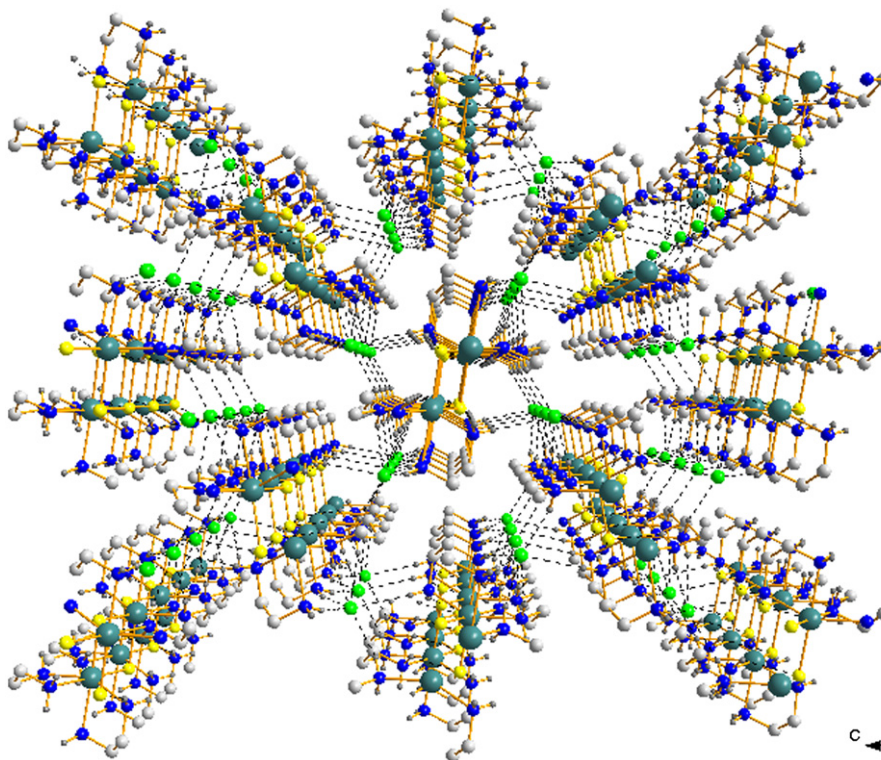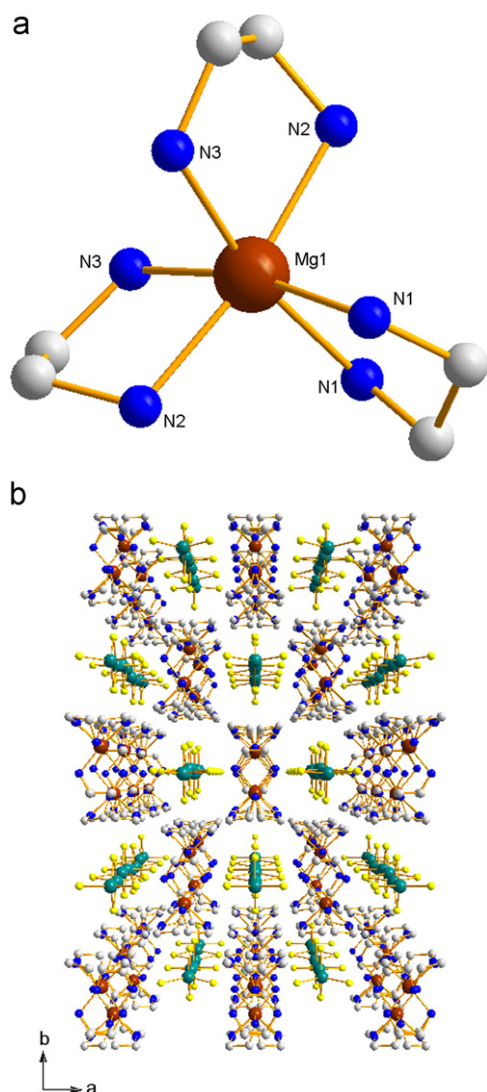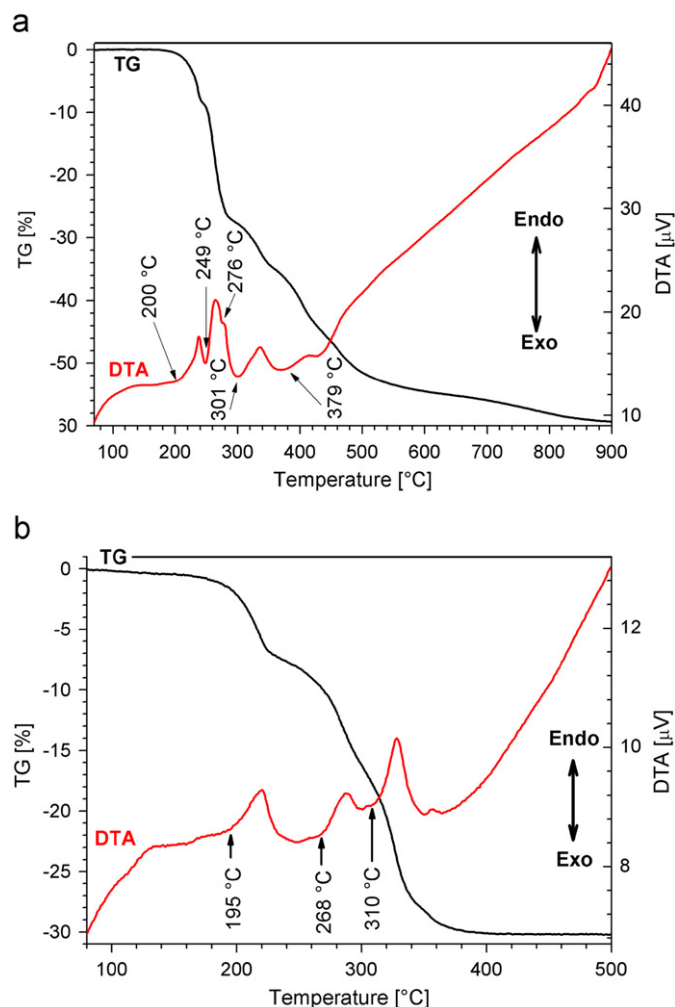**Fig. 3.** 3-D framework made by linking the zero-dimensional thioindates through N–H···S and N–H–Cl H-bonds.

Fig. 5. (a) View of the $[Mg(en)_3]^{2+}$ complex in **2**. (b) 3-D view of the structure of **2**. The 1-D $\{[InS_2]^-\}_\infty$ chain running parallel to the [001] direction.

Fig. 6. DTA/TG curves of (a) **1**, (b) **2**.

explanation of the different thermal events is not possible without simultaneous mass spectrometry measurements. The total mass loss until 500 °C is about 51.5%, close to the expected value for the emission of the amine and Cl (expected: 51.4%), and formally the binary sulphide InS is formed. As can be seen in Fig. 6a, the mass loss is not finished at the 500 °C and some organic contamination (see Section 2) as well as some chlorine remains in the residue. The presence of Cl in the residue was corroborated by EDX measurements (Fig. S3, supporting information). The chemical composition of some white microparticles at the surface of the product after thermal decomposition was determined with EDX to In:Cl=1:3, suggesting that $InCl_3$ was formed during the thermal decomposition processes. The powder pattern of the product obtained at 500 °C (Fig. 8b, see below) evidences the formation of α-In_2S_3. This observation supports the assumption that the thermal decomposition is more complex than expected by comparing the experimental and theoretical mass losses. Increasing the temperature to 900 °C an additional mass loss is observed yielding the final value of about 59.4%. It can be assumed that in the temperature range from 500 to 900 °C remaining organic contaminants as well as the In chloride are emitted. The powder pattern of the residue (Fig. 8b) suggests the formation of β-In_2S_3 (see next).

The TG curve of **2** displays three well resolved steps accompanied by three endothermic peaks in the DTA curve at about 195, 268 and 310 °C (T_{onset} values). The total mass loss until 500 °C is about 30.2%, and 1.8% less than expected for the emission of the amine molecules (expected: 32%). The chemical analysis of the residue revealed the presence of some C and N (see Section 2) explaining the difference between expected and measured mass loss. The observation that some organic material remains in a decomposition product is not surprising because the organic molecules may undergo fragmentation during thermal reactions and the residue is contaminated by fragments of the organic material. The presence of slight contamination is often observed if thiometallates containing organic molecules are thermally decomposed in inert atmosphere [34–37].

4.2. Optical properties

The Kubelka–Munk plots for the determination of the optical band gaps of **1** and **2** are shown in Fig. 7(a) and (b), respectively. In the curve α^2/s^2 is plotted against energy with α being the absorption coefficient and s the scattering coefficient [38]. The optical band gap of the compounds was determined to $E_g=3.47$ (**1**) and $E_g=3.59$ eV (**2**). Because these values are very similar the absorption edge may be assigned to electronic transitions between levels of the In and S atoms. The In–S–In angles and the In–S bond-lengths in both compounds are very similar with
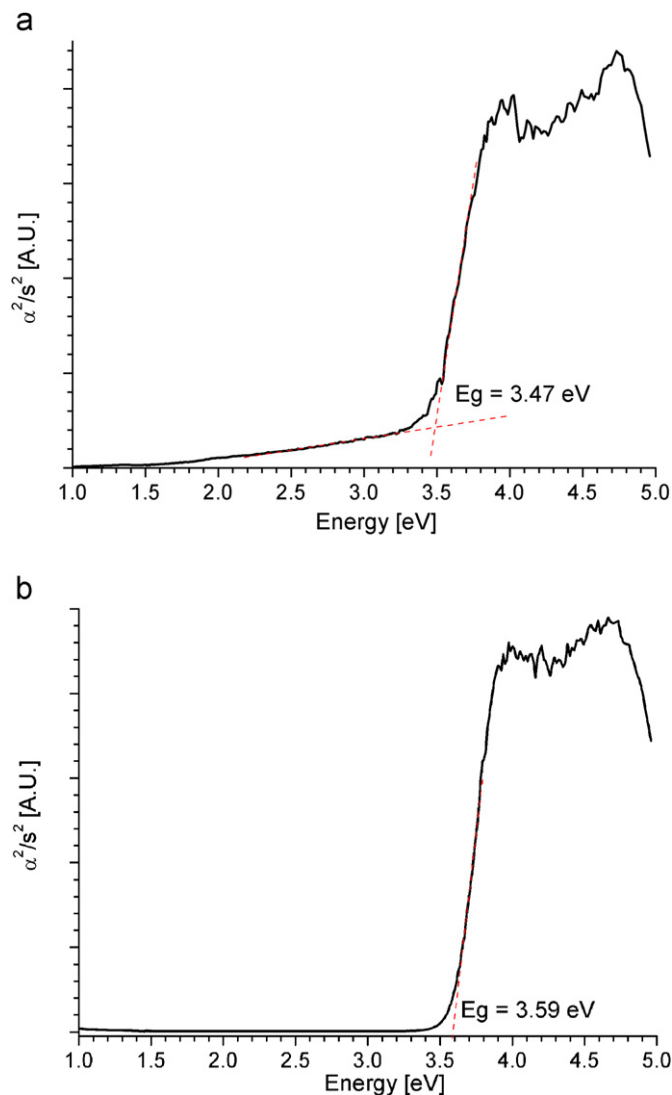
Fig. 7. Kubelka–Munk plots for the determination of the optical band gap of (a) **1** and (b) **2**.

Fig. 8. (a) X-ray powder diffractograms of decomposition products of compounds **1** obtained at 500 °C (**1x**) and **2x** together with the calculated diffractograms of α-In_2S_3 and $MgIn_2S_4$ displayed for comparison. (b) X-ray powder patterns of **1x** and of the residue obtained at 900 °C.

small differences (see Tables 2 and 3), which may account for the slightly differing values for E_g.

5. Structural characterization of the decomposition products

The X-ray powder diffractograms (PDs) of **1x** and **2x** are shown in Fig. 8a. The reflections in the powder pattern of **1x** match well with those of the pattern of α-In_2S_3 (cubic) [39] and the absence of the (112) reflection at about 17° 2θ of β-In_2S_3 [40] indicates the that the cubic modification is formed at 500 °C during the thermal decomposition process.

In the powder pattern of the residue obtained at 900 °C some weak reflections in the low angle region suggests the presence of β-In_2S_3 (Fig. 8b, marked region). The occurrence of reflections of the β-modification indicates some loss of In because this phase is more stoichiometric than the α-phase (see below).

The size of the coherent scattering domains in the sample **1x** was evaluated applying the Scherrer equation. The quantification yields about 29 nm for the most intense reflection. α-In_2S_3 is a high temperature modification of In_2S_3 and according to data presented in the literature this modification can be stabilized at room temperature in the presence of an In excess [41]. In the case
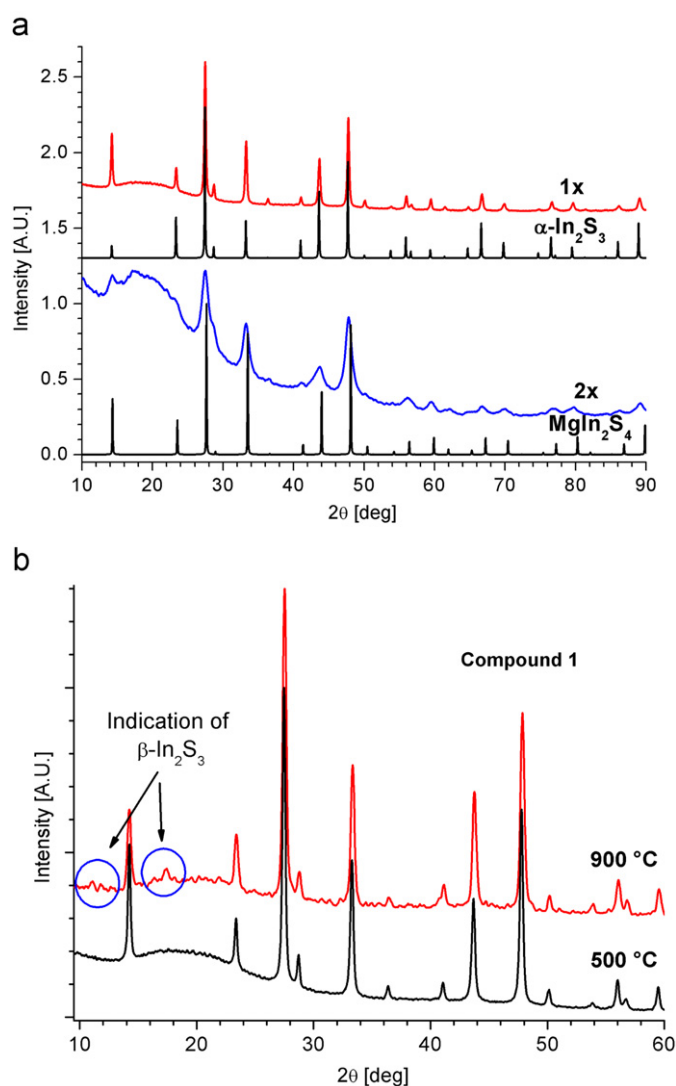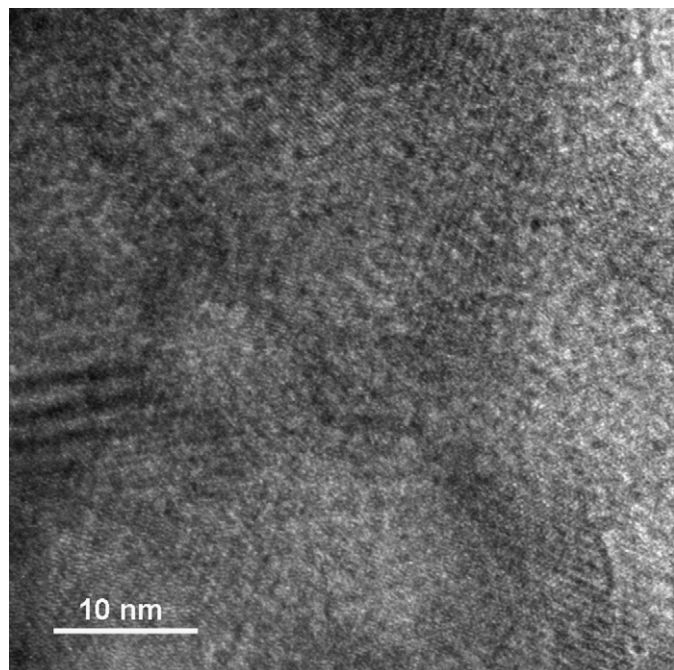
of **1x** the formation of α-In_2S_3 seems to be reasonable because it is obtained from an In-rich precursor compound with In:S = 1:1, and stoichiometric In_2S_3 would require the removal of one-third of In. According to literature data the α-phase is stable with the composition $In_{2+x}S_3$ (0.01 < x < 0.18) [41]. But there is also a report where the α-modification was obtained for very small deviation of the exact stoichiometry [42]. Additionally In–S films having an In/S ratio between 0.79 and 0.94 have been described as a combination of the α- and β-modifications [43]. The amount of $InCl_3$ in **1x** is either too small to be detected in the powder pattern or the compound is amorphous. Nevertheless, the formation of $InCl_3$ reduces the In:S ratio and the nonstoichiometric α-In_2S_3 modification is formed during the thermal decomposition process stopped at 500 °C.

The diffraction pattern of **2x** can be explained on the basis of the cubic spinel-type structure of $MgIn_2S_4$ [44]. Because no additional crystalline phases were detected in the pattern the remaining organic components must be amorphous. The presence of Mg, In and S in the 1:2:4 ratio was confirmed with the EDX analysis (Fig. S3, supporting information). The reflections of the decomposition product are significantly broadened, which is
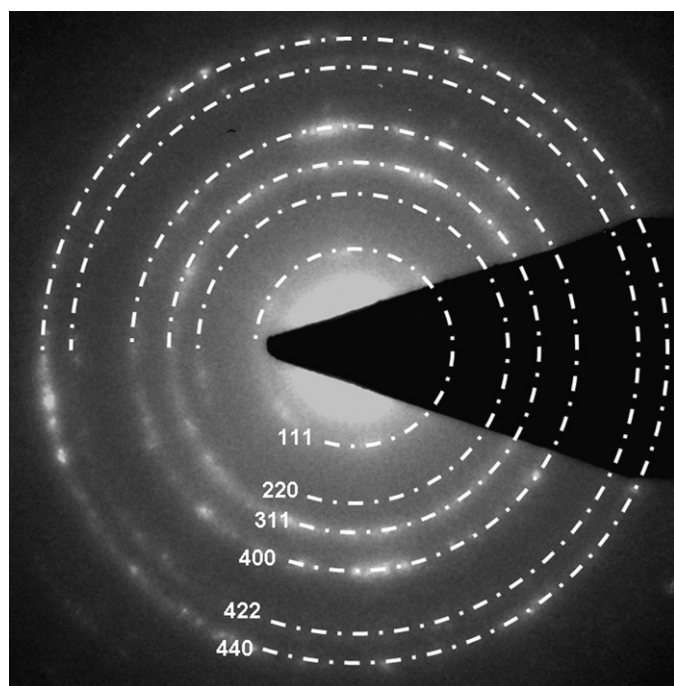
caused by particle size effects. The average particle size calculated with the Debye–Scherrer formula using the most intense reflections (no correction was made for instrumental broadening) is about 9 nm, evidencing the nanocrystalline nature of this material.

The TEM micrographs of **2x** show that the sample is composed of nanocrystals randomly oriented (Fig. 9) separated by thin amorphous regions possibly composed of the organic residue. The electron diffraction patterns (ED) recorded inside selected areas of

Table 4
List of d-values in the ED pattern of sample **2x** (Å).

2x	MgIn$_2$S$_4$	h k l
6.2	6.17	(111)
3.88	3.78	(220)
3.27	3.22	(311)
2.69	2.67	(400)
2.14	2.18	(422)
1.9	1.88	(440)

the nanosized crystals can be indexed assuming the structure of MgIn$_2$S$_4$ [44], as specified in Fig. 10. The *d* values calculated from the ED pattern are summarized in Table 4. The presence of reflections on concentric circles confirms random orientation of the crystalline grains.

6. Conclusions

A zero- (compound **1**) and a one-dimensional (compound **2**) thioindate have been prepared under solvothermal conditions. Compound **1** consists of isolated complexes linked via H-bonding interactions and represents the first example for a cationic thioindate. The structure of compound **2** contains linear $\{[InS_2]^-\}_\infty$ chains, charge compensated by $[Mg(en)_3]^{2+}$ complexes. Like in compound **1** an extended hydrogen bond network is observed to form a three-dimensional S···H connected network. We note that examples of thiometallates with complexes of earth-alkaline metal complexes are rare and were only reported for a thioantimonate(III) compound [33]. The optical band-gaps of **1** and **2** are very similar demonstrating the small influence of the charge compensating counterparts. Therefore, it is most likely that the absorption is due to electronic transitions between In based and S atom based atomic levels. The thermal reactivity of the two compounds is complex and totally different. For **1** the thermal decomposition is not finished at 500 °C whereas for **2** no weight loss is observed above about 400 °C until the final temperature of 500 °C. During the thermal decomposition reaction of **1** the cubic modification α-In$_2$S$_3$ is formed at 500 °C despite the starting In:S ratio of 1:1. This observation demonstrates that the thermal decomposition is much more complex than the simple emission of the en molecules and Cl. The X-ray powder pattern of the residue obtained at 900 °C suggests the crystallization of β-In$_2$S$_3$. The thermal decomposition product of compound **2** was identified as nanocrystalline MgIn$_2$S$_4$ crystallizing in the spinel-type structure.

Acknowledgments

Appendix A. Supplementary materials

Supplementary data associated with this article can be found in the online version at doi:10.1016/j.jssc.2010.09.024.

Fig. 9. Typical TEM micrograph of **2x**. The sample is composed of MgIn$_2$S$_4$ nanocrystals randomly oriented.

Fig. 10. Electron diffraction pattern of a selected area of **2x**. The observed rings can be indexed with the cubic structure of MgIn$_2$S$_4$.

References

[1] P. Feng, X. Bu, N. Zheng, Acc. Chem. Res. 38 (2005) 293.
[2] N. Zheng, X. Bu, P. Feng, Angew. Chem. 116 (2004) 4857.
[3] Q. Zhang, X. Bu, L. Han, P. Feng, Inorg. Chem. 45 (2006) 6684.
[4] N. Zheng, X. Bu, H. Lu, L. Chen, P. Feng, J. Am. Chem. Soc. 127 (2005) 14990.
[5] C.L. Cahill, B. Gugliotta, J.B. Parise, Chem. Commun. (1998) 1715.

[6] C. Wang, X. Bu, N. Zheng, P. Feng, Angew. Chem. Int. Ed. 41 (2002) 1959.

[7] P. Vaqueiro, J. Solid State Chem. 179 (2005) 302.

[8] J. Zhou, G.Q. Bian, Y. Zhang, Q.Y. Zhu, C.Y. Li, J. Dai, Inorg. Chem. 46 (16) (2007) 6347.

[9] C.Y. Li, J. Zhou, Y. Zhang, Z.X. Lei, G.Q. Bian, J. Dai, Z. Anorg. Allg. Chem. 635 (2009) 151.

[10] T.T. John, M. Mathew, C.S. Kartha, K.P. Vijayakumar, T. Abe, Y. Kashiwaba, Sol. Energy Mater. Sol. Cells 89 (2005) 27.

[11] N. Kamoun, S. Belgacem, M. Amlouk, R. Bennaceur, J. Bonnet, F. Touhari, M. Nouaoura, L. Lassabatere, J. Appl. Phys. 89 (5) (2001) 2766.

[12] S.H. Choe, T.H. Bang, N.O. Kim, H.G. Kim, C.I. Lee, M.S. Jin, S.K. Oh, W.T. Kim, Semicond. Sci. Technol. 16 (2001) 98.

[13] D.K. Nagesha, X. Liang, A.A. Mamedov, G. Gainer, M.A. Eastman, M. Giersig, J.J. Song, T. Ni, N.A. Kotov, J. Phys. Chem. B 105 (2001) 7490.

[14] N. Barreau, J.C. Bernède, C. Deudon, L. Brohan, S. Marsillac, J. Cryst. Growth 241 (2002) 4.

[15] N. Barreau, C. Deudon, A. Lafond, S. Gall, J. Kessler, Sol. Energy Mater. Sol. Cells 90 (2006) 1840.

[16] N. Barreau, Sol. Energy 83 (2009) 363.

[17] Y. Xing, H. Zhang, S. Song, J. Feng, Y. Lei, L. Zhao, M. Li, Chem. Commun. (2008) 1476.

[18] Y. He, D. Li, G. Xiao, W. Chen, Y. Chen, M. Sun, H. Huang, X. Fu, J. Phys. Chem. C 113 (2009) 5254.

[19] Y. Xiong, Y. Xie, G. Du, X. Tian, J. Mater. Chem. 12 (2002) 98.

[20] X. Cao, L. Gu, L. Zhuge, W. Qian, C. Zhao, X. Lan, W. Sheng, D. Yao, Colloids Surf. A: Physicochem. Eng. Aspects 297 (2007) 183.

[21] D.P. Dutta, G. Sharma, A.K. Tyagi, S.K. Kulshreshtha, Mater. Sci. Eng. B 138 (2007) 60.

[22] H.X. Bai, L.X. Zhang, Y.C. Zhang, Mater. Lett. 63 (2009) 823.

[23] W. Chen, J.O. Bovin, A.G. Joly, S. Wang, F. Su, G. Li, J. Phys. Chem. B 108 (2004) 11927.

[24] K.H. Park, K. Jang, S.U. Son, Angew. Chem. 118 (2006) 4724.

[25] G.M. Sheldrick, Acta Crystallogr. A 64 (2008) 112.

[26] E. Quiroga-González, C. Näther, W. Bensch, Solid State Sci. 12 (2010) 1235.

[27] D. Pitzschke, W. Bensch, Angew. Chem. 115 (2003) 4525.

[28] S. Abram, C. Maichle-Mossmer, U. Abram, Polyhedron 17 (1998) 131.

[29] D.L. Reger, P.S. Coan, Inorg. Chem. 34 (1995) 6226.

[30] D. Pitzschke, C. Näther, W. Bensch, Solid State Sci. 4 (2002) 1167.

[31] E. Zintl, K. Loosen, Z. Phys. Chem. 174 (1935) 301.

[32] S.S. Dhingra, R.C. Haushalter, Chem. Mater. 6 (1994) 2376.

[33] E. Quiroga-González, C. Näther, W. Bensch, Z. Naturforsch. 64b (2009) 1312.

[34] V. Spetzler, H. Rijnberk, C. Näther, W. Bensch, Z. Anorg. Allg. Chem. 630 (2004) 142.

[35] M. Schaefer, D. Kurowski, A. Pfitzner, C. Näther, Z. Rejai, K. Möller, N. Ziegler, W. Bensch, Inorg. Chem. 45 (2006) 3726.

[36] V. Spetzler, C. Näther, W. Bensch, Inorg. Chem. 44 (2005) 5805.

[37] B.R. Srinivasan, S.N. Dhuri, C. Näther, W. Bensch, Inorg. Chim. Acta 358 (2005) 279.

[38] D. Gal, Y. Mastai, G. Hodes, J. Appl. Phys. 86 (10) (1999) 37.

[39] C. Adenis, J. Olivier-Fourcade, J.C. Jumas, E. Philippot, Rev. Chim. Min. 24 (1987) 10.

[40] G.A. Steigmann, H.H. Sutherland, J. Goodyear, Acta Crystallogr. 19 (1965) 967.

[41] R. Diehl, R. Nitsche, J. Cryst. Growth 28 (1975) 306.

[42] N. Revathi, P. Prathap, K.T. Ramakrishna Reddy, Appl. Surf. Sci. 254 (2008) 5291.

[43] R. Bayón, J. Herrero, Appl. Surf. Sci. 158 (2000) 49.

[44] H. Hahn, W. Klingler, Z. Anorg. Allg. Chem. 263 (1950) 177.